Electrolyzer models for hydrogen production from wind energy systems

Raúl Sarrias-Mena, Luis M. Fernández-Ramírez, Carlos Andrés García-Vázquez, Francisco Jurado

Published in:
International Journal of Hydrogen Energy, vol. 40, nº 7, pp. 2927-2938

DOI (link to publication from Publisher):
https://doi.org/10.1016/j.ijhydene.2014.12.125

Publication date:
2015

Document Version:
Accepted version

Elsevier Editorial System(tm) for International Journal of Hydrogen Energy
Manuscript Draft

Manuscript Number: HE-D-14-03066R1

Title: Electrolyzer models for hydrogen production from wind energy systems

Article Type: Full Length Article

Section/Category: Solar Hydrogen / Renewable Hydrogen

Keywords: Electrolyzer; hydrogen; modelling; wind turbine.

Corresponding Author: Dr. Luis M. Fernandez, Ph. D.

Corresponding Author's Institution: University of Cadiz

First Author: Raul Sarrias-Mena, M.Sc.

Order of Authors: Raul Sarrias-Mena, M.Sc.; Luis M. Fernandez, Ph. D.; Carlos Andrés García-Vázquez, Ph. D.; Francisco Jurado, Ph. D.

Abstract: The continuous progress on the expansion of renewable energies leads to the development of hybrid power systems, where several power sources contribute to provide a clean and reliable alternative to traditional fossil fuels. The hydrogen technology is viewed with particular interest in this regard. Hydrogen is an outstanding energy carrier that can be exploited for various applications, including electricity generation. Hence, production of hydrogen from renewable sources has received the attention of many researchers lately. With this purpose, this paper deals with the coupled operation of electrolyzer (EZ) and wind turbine. Four different EZ models are presented and evaluated in this work. These models are aggregated to a variable speed wind turbine model using MATLAB/Simulink. The four configurations are evaluated, and their responses compared, under variable wind speed and grid demand.

Highlights

- Four electrolyzer models for hydrogen production from wind energy systems were compared.
- The coupled operation of electrolyzer and wind turbine was evaluated.
- The decision to use one model relies on the characteristics of the application under study.

Electrolyzer models for hydrogen production from wind energy systems

Raúl Sarrias-Mena [1], Luis M. Fernández-Ramírez [1,*], Carlos Andrés García-Vázquez [1], Francisco Jurado [2]

[1] *Research Group in Electrical Technologies for Sustainable and Renewable Energy (PAIDI-TEP-023), Department of Electrical Engineering, University of Cadiz, 11202 EPS Algeciras, Algeciras (Cadiz), Spain*

[2] *Research Group in Research and Electrical Technology (PAIDI-TEP-152), Department of Electrical Engineering, University of Jaen, 23700 EPS Linares, Linares (Jaen), Spain*

Abstract

The continuous progress on the expansion of renewable energies leads to the development of hybrid power systems, where several power sources contribute to provide a clean and reliable alternative to traditional fossil fuels. The hydrogen technology is viewed with particular interest in this regard. Hydrogen is an outstanding energy carrier that can be exploited for various applications, including electricity generation. Hence, production of hydrogen from renewable sources has received the attention of many researchers lately. With this purpose, this paper deals with the coupled operation of electrolyzer (EZ) and wind turbine. Four different EZ models are presented and evaluated in this work. These models are aggregated to a variable speed wind turbine model using MATLAB/Simulink. The four configurations are evaluated, and their responses compared, under variable wind speed and grid demand.

* Corresponding author. Tel.: +34 956 028166; fax: +34 956 028001.
E-mail addresses: raul.sarrias@uca.es (R. Sarrias-Mena), luis.fernandez@uca.es (L. M. Fernández-Ramírez), carlosandres.garcia@uca.es (C. A. García-Vázquez), fjurado@ujaen.es (F. Jurado).

Keywords.

Electrolyzer; hydrogen; modelling; wind turbine.

1. Introduction

Renewable energy systems experience continuous advances pursuing higher power rates, improved efficiency, reduced impact on electric power systems, etc. Nowadays, many studies are trending towards hybrid configurations, with several energy sources working co-ordinately [1-3]. As a main advantage, the hybrid option aggregates the prime qualities of all the elements involved. Subsequently, the weaknesses of each individual component can be minimized and compensated by the characteristics of other devices [4]. Following this concept, hybrid power systems based on wind energy as the main source have been evaluated in the literature [5, 6]. Given the natural origin of the power source, wind generation is often intermittent and unpredictable. Additionally, it cannot be handled on demand, since favourable wind conditions are required. Hence, it is possible to bear situations when an excess of wind generation is wasted as it cannot be absorbed by the grid, as well as many other circumstances with low wind power production during a peak on demand. The ability to store the energy surpluses in the adequate devices greatly improves the performance of wind power systems, thus enhancing their grid penetration under more reliable conditions.

Different energy storage systems (ESSs) are considered adequate for coupled operation with renewable energy sources. Depending on the technology, some characteristics prevail over others. For instance, several battery types are well developed for large scale energy storage in the range of hours [7, 8], whereas ultracapacitors or

superconducting magnetic energy storage are better suited for very fast power exchange applications [5, 8, 9]. The hydrogen technology appears as an exceptional long-term storage alternative in the so-called power-to-gas plants [10]. Alternative technologies based on the storage of energy in the form of heat are also interesting options for the long-term, especially for energy infrastructures with a large participation of fluctuating renewable sources and combined heat and power (CHP) production systems [11]. In this regard, heat pumps and/or electric boilers can use the excess electricity provided by renewable sources to produce heat that can be conserved in a heat storage [11], thus reducing the need for consuming fossil fuels for heat generation while increasing the flexibility of the system to supply the electricity and heat demands. Likewise, EZs may play a relevant role in this generation scheme, since they can use the excess electric power from renewable sources to produce hydrogen for the CHP system [11]. Additionally, pumped hydro and compressed air energy storage appear as two valid choices for large-scale storages, which are also able to curtail generation surpluses from wind power. Nonetheless, these are usually handicapped by the particular characteristics required on the installation site [7].

The excess energy generation from renewable sources can be utilized to produce hydrogen in an EZ. The obtained hydrogen can be stored in various ways, and eventually employed in fuel cells to deliver electric energy. This option offers a practically inexhaustible supply of clean energy, since the tanks where hydrogen is stored can accumulate high quantities of this element. Moreover, they can be emptied and the hydrogen transported to a different location. Hence, the EZ can operate continuously with almost inexistent storage boundaries. However, the applications of the hydrogen obtained from EZs are not limited to electricity production in fuel cells. Alternatively, this element can be used as a raw material in the synthesis of renewable

transport fuels by combination of hydrogen with carbon obtained from recycled CO_2 or biomass [12, 13]. The use of hydrogen in these applications provides a dual benefit: firstly, it reduces the amount of biomass (which is a limited resource) needed to produce clean fuels; and secondly, it adds flexibility to the electric power system, thus allowing a higher integration of intermittent renewable sources [12]. Such renewable fuels are expected to gain great importance in the development of future transport systems based on clean sources [12], since they can overcome some of the problems related to the production of biofuels, thus rising as a supplement or substitute for them in scenarios with high rates of renewable energies [13]. The growth of this industry demands a further evolution of EZs [13]. Due to this flexibility, as well as the variety of applications and potential utilization of the product delivered, an EZ has been chosen as energy storage device in the hybrid system considered in this paper.

The implementation of EZ in hybrid power systems with renewable sources has been addressed in the literature from various perspectives. Coupled operation with solar photovoltaic systems was dealt in [14, 15]. In both cases, a stand-alone application including fuel cells was investigated, thus not influencing the activity of a large power system. How the hydrogen technology improved the integration of wind generation was studied as an optimization problem in [16]. An optimal power flow routine maximized the wind power injection to grid, with the singularity that a certain external hydrogen demand must be satisfied meanwhile. Several costs involved in the operation of the hybrid system were considered, and the wind farm was modelled through equality constraints to the optimal solution, thus neglecting their dynamic performance. Zhou *et al.* presented in [17] an EZ model and control strategy for a hybrid configuration, including the necessary power converters. Moreover, a hardware-in-the-loop simulation was carried out to test the proposed models. Nonetheless, the wind turbine dynamics

were not considered, thus not being able to observe the overall response of the hybrid configuration and the total power exchange with the grid. An actual hybrid demonstration plant was evaluated in [18] using registered data from the installation deployed in Utsira, Norway. The most interesting results of their study were discussed, whereas the modelling process of the power sources and auxiliary equipment was not introduced. Carton and Olabi [19] raised the challenge to develop a hybrid pilot plant in Ireland, similarly to that implemented in [18]. The authors listed the many benefits of such hybrid configurations, and protested the necessity to improve the capacity of the Irish power system, proposing the hybrid wind/hydrogen configuration as a viable solution. A complete hydrogen micro-system including EZ, hydrogen storage and fuel cell was used in [20] to support grid integration of a wind generator. A thorough depiction of the control systems was carried out. However, low power devices were considered, also disregarding the description of their modelling process. Hydrogen production systems can also provide frequency regulation support to wind farms, as reported in [21]. Smoothing the output power of a wind farm via hydrogen generation was contemplated in [22]. A line power reference was determined for the wind farm, being the EZ devices responsible for absorbing the excess power. Such strategy reduced the switching operation of the EZ, but the grid demand was not considered as an input in the control scheme.

So far, a study with a similar approach to that accomplished herein has not been carried out. The main motivation of this paper is to develop a comparative analysis of four different EZ models presented in the literature. In most of the cases, researchers put their focus on the design, description and simulation of new or improved EZ models. Therefore, the evaluation of these models as a part of a more complex energy system is often neglected. This is especially true in the case of detailed proton exchange

membrane (PEM) EZ models. As a consequence, this article aims at drawing attention to the coupled operation of PEM EZ models with other renewable energy sources, as is the case with wind power. Hybridization of wind energy systems by using EZ devices as energy storage optimizes the energy capture of such renewable source, and thus its overall performance. Hence, it is worth increasing the existing knowledge on the coordination and the energy management within all the elements required in this type of hybrid power systems. Four EZ models, with diverse degree of complexity, have been chosen for this study. They have been integrated within a doubly-fed induction generator (DFIG) based wind generator. A supervisory control system (SCS) is in charge of managing the energy exchange, thus coordinating the coupled operation of both devices. In order to evaluate and compare the response of the EZ models, these hybrid systems have been simulated under fluctuating wind speed and variable grid power requirements.

The rest of the paper is structured as follows. The modelling of the wind energy system is depicted in Section 2. Section 3 provides a detailed description of the EZ models considered in this study. In Section 4, the implementation of the hybrid system through the necessary control strategies is explained. Simulation results are discussed in Section 5, and finally Section 6 expounds the main conclusions.

2. Wind energy system modelling

The wind energy system forms the principal power source in the hybrid system. As its main duties, the wind turbine must capture the kinetic energy of the incoming wind while circulating the excess power to the EZ. A 1.5 MW DFIG-driven wind turbine has been considered for these purposes. This element has been modelled according to the

characteristics of a product commercialized by General Electric [23], in order to achieve a higher accuracy in the results.

The DFIG-based wind power system has been modelled in MATLAB/Simulink. Well-known models have been implemented for the wind turbine and electric generator. Therefore, these are only briefly outlined herein. A more thorough depiction can be found in our previous works [24, 25]. The description of the pitch angle and DFIG converter controllers that govern the behaviour of the wind power system is also addressed.

2.1. Wind turbine

Traditionally, the actuator disk theory detailed in [26] is used to model the dynamic response of the wind turbine, comprised by the blades coupled to the hub. This simple model allows calculating the mechanical torque produced in the wind turbine rotor and transmitted to the DFIG rotor through the drive train. The two-mass dynamic model [27] has been used to represent this mechanical system including the wind turbine and electric generator rotors, linked by the gearbox in the drive train. This model outputs the mechanical torque of the DFIG rotor, which is necessary in the DFIG model.

2.2. Doubly-fed induction generator

The DFIG is a very popular choice in wind power systems nowadays. This electric generator offers a wide speed variation range, as well as the capacity to control active and reactive power generation independently. This independent power regulation can be achieved by means of the power converter implemented to connect the rotor windings to grid, which consists of two back-to-back bridges, namely Rotor Side Converter and Grid Side Converter (i.e.: RSC and GSC), linked by a DC bus. An active crowbar has also been included to disconnect the power converter in case of rotor overcurrent during

grid faults. On the other hand, the stator windings are directly connected to grid, thus assuming its frequency and voltage level.

A detailed fifth-order model has been considered for the DFIG [28]. Hence, four differential equations for the electric variables, plus the expression for the electromechanical torque, are used. The electric equations correspond to the stator and rotor voltage, expressed in the direct-quadrature (*dq*) reference frame rotating at synchronous speed. These *d*-*q* components are expressed as a function of the rotor and stator electrical resistance, and the magnetic flux linkages. The stator and rotor voltages play a crucial role in the control strategy implemented on the DFIG power converter, as it will be shown later on.

2.3. Pitch angle controller

The wind power system is equipped with a pitch angle controller to regulate the rotating speed of the wind turbine. When the angular speed exceeds the reference value, the pitch angle of the blades increases to reduce the aerodynamic wind power capture, thus driving the wind turbine back to its rated speed. Conversely, the pitch angle is set to zero for rotating speeds below the nominal value, in order to maximize the wind power transformation in the wind turbine. This control strategy has been implemented in this model through a single control loop based on a PI controller. The slow dynamics of the pitch angle actuator have also been considered, so that a progressive variation of the angle can be achieved.

2.4. Rotor side converter controller

In the control strategy implemented, the RSC regulates the total active power generation of the DFIG (P_g) and the stator reactive power exchange (Q_s) independently. This can be accomplished through decoupled vector control, by acting on the *d*-*q*

components of the rotor voltage. Two separate PI-based double control loops are used for this purpose. The outer control loops determine the *d-q* rotor current references that regulate the controlled parameter (i.e: P_g and Q_s for the *d* and *q* components respectively). Then, the current references are converted to the *d-q* rotor voltages in the inner control loops. The *d-q* components of the rotor voltage are inputted to the PWM converter that generates the trigger signal for the power switches in the RSC.

The references for P_g and Q_s are externally calculated in the SCS according to a coordinated global control strategy for the hybrid system, and then inputted to the RSC controller.

2.5. Grid side converter controller

Decoupled vector control has also been implemented on the GSC controller. Here, the DC bus voltage of the power converter (V_{dc}) has been controlled through the *d* component of the grid side voltage, whereas the *q* component has been used to regulate the reactive power exchange in this converter (Q_{gsc}). In accordance with the scheme implemented on the RSC, two analogous PI-based double control loops have been considered. The outer control loops follow the V_{dc} and Q_{gsc} references by generating the *d* and *q* components of the grid side current respectively with PI controllers. Then, the inner control loops calculate the *d-q* components of the grid side voltage in order to achieve the current references. Finally, a PWM generator receives the *d-q* grid side voltage and outputs the trigger signal for the power switches in the converter.

In the GSC, the V_{dc} reference is set to a constant value of 2000 V, whereas Q_{gsc} is provided by the SCS according to the varying conditions of the grid demand, as it will be stated later on.

3. PEM electrolyzer modelling

In the literature, there exist various alternatives for the modelling of a PEM EZ. Generally, only two parameters are crucial when the response of an EZ model is evaluated: the polarization curve (i.e.: variation of voltage with current or current density in the EZ), and the hydrogen production. Other magnitudes, such as temperature and pressure in anode, cathode or membrane, are also relevant to understand the performance of this device; but they are sometimes neglected for the sake of simplicity in the model. In this paper, four different options have been considered. The EZ models studied present a dissimilar degree of complexity and detail, as it will be described below.

3.1. Electrolyzer model A

In commercial EZ devices, the ratio between voltage and current can be considered constant for most of the polarization curve. As a consequence, the EZ voltage can be expressed as a linear function of the input current. This performance resembles that of an electrical resistance, which is the concept applied on this model. Hence, the electrical response of the model A is modelled through a DC voltage source and a series-connected electrical resistance. The function of the DC voltage source is to introduce the zero-current voltage of the EZ, whereas the series resistance models the direct variation of voltage with an increase in the input current. Both the voltage source and resistance values must be determined through observation of a polarization curve of the device. Therefore, these parameters must be adjusted according to the characteristics of the EZ. Moreover, the influence of pressure and temperature is neglected in this model. This implies that the model loses accuracy for pressure or temperature conditions

different to that illustrated in the polarization curve chosen as a reference. Alternatively, the DC voltage and resistance can be re-calculated for a new polarization curve obtained under the modified pressure and temperature. As seen, this behaviour allows great simplicity in the model, although it lacks of versatility for variable pressure and temperature.

Regarding the hydrogen production in the EZ, the Faraday's law has been utilized to calculate this parameter [29, 30]. As seen in Eq. (1), the output hydrogen flow (n_{H2}) is directly proportional to the current through the EZ and the number of series cells (I_{EZ} and n_c respectively), divided by two times the Faraday constant (F). Furthermore, an efficiency factor must be used to account for the deviation of the model from the ideal performance. Hence, the Faraday efficiency (η_F) is used in Eq. (1). This parameter is commonly calculated in the literature as in Eq. (2), assuming that the EZ temperature is maintained at a constant value during its operation.

$$n_{H2} = \frac{n_c \cdot I_{EZ}}{2 \cdot F} \cdot \eta_F \tag{1}$$

$$\eta_F = 96.5 \cdot exp\left(\frac{0.09}{I_{EZ}} - \frac{75.5}{I_{EZ}^2} \right) \tag{2}$$

Through (1) and (2), plus the electrical modelling as a resistor, the model A for a commercial EZ is complete, providing the basic dynamic operation information of this equipment.

3.2. Electrolyzer model B

Similarly to the previously described model, the concept of the linear variation of voltage and current is also used in model B. Moreover, this model also deals with the pressure and temperature variations at the EZ. As a consequence, once the model is properly adjusted, it is able to reproduce the polarization curve of a real device for different pressure and temperature conditions, without the necessity to modify any parameter of the model.

The voltage response of this model (V_{EZ}) is calculated upon two terms [31], as shown in Eq. (3). The first term corresponds to the zero-current voltage, whereas the second is current-dependent. In both cases, the effect of temperature and pressure are regarded.

$$V_{EZ}\left(T,p\right)=e_{rev}\left(T,p\right)+I_{EZ}\cdot R_i\left(T,p\right) \tag{3}$$

This simple EZ model has been built through the minimum voltage that allows a current flow in the EZ, namely *reverse voltage* or e_{rev}, and the internal resistance of the device R_i, which defines the variation of the EZ current (I_{EZ}) with changes in the input voltage. The main particularity of this model relies on the inclusion of the pressure (p) and temperature (T) effects. This can be achieved by defining both the reverse voltage and the internal resistance as in Eqs. (4) and (5) respectively [31].

$$e_{rev}\left(T,p\right)=e_{rev0}+\frac{R\cdot T}{2\cdot F}\cdot\ln\left(\frac{p}{p_0}\right) \tag{4}$$

$$R_i\left(T,p\right)=R_{i0}+k\cdot\ln\left(\frac{p}{p_0}\right)+dR_t\cdot\left(T-T_0\right) \tag{5}$$

Some parameters are necessary in order to implement Eqs. (4) and (5) in the dynamic EZ model. R is the ideal gas constant expressed in $l \cdot atm \cdot K^{-1} \cdot mol^{-1}$. The reference values for the reverse voltage, internal resistance, pressure and temperature are given in Eqs. (4)-(5) as e_{rev0}, R_{i0}, p_0 and T_0 respectively. The curve fitting parameter k is also implemented in Eq. (5), together with the resistance coefficient of temperature dR_t. These parameters have been sized as in [31], and then slightly modified to adapt to the characteristics of the commercial device employed in this paper when necessary. Eventually, the EZ voltage in Eq. (3) is modified according to the number of series and parallel branches considered in the dynamic model.

Regarding the hydrogen production, it can be obtained from the EZ current, pressure and temperature, as given in Eq. (6). This parameter is also proportional to the number of series cells in the device, n_c.

$$n_{H2}(T, p) = \frac{T \cdot R}{p} \cdot \frac{I_{EZ}}{2 \cdot F} \cdot n_c \tag{6}$$

The previous set of equations completely describes the EZ model B implemented and evaluated in this study.

3.3. Electrolyzer model C

A more complex EZ model has been chosen as model C in the comparative analysis. It is based upon the model presented in [32], which takes into consideration the electrochemical performance of different elements in this device, thus providing more detail concerning its internal parameters.

Dynamic model C is divided into four different elements, namely the anode, cathode, membrane and voltage ancillaries. In each of them, a set of equations represents the electrochemical response of certain variables. A short description of this model is depicted herein.

The partial pressures of oxygen and hydrogen (p_{O2} and p_{H2}) are calculated through Eqs. (7) and (8) in the anode and cathode ancillaries respectively, and then inputted to the voltage ancillary. They also allow calculating the oxygen and hydrogen molar fractions, which are required in order to compute the molar and volumetric flows of these elements.

$$p_{O2} = \frac{N_{O2} \cdot R \cdot T}{V_a} \tag{7}$$

$$p_{H2} = \frac{N_{H2} \cdot R \cdot T}{V_c} \tag{8}$$

N_{O2} and N_{H2} are the moles of oxygen and hydrogen at the anode and cathode, which are obtained through mass balance in both structures. Moreover, V_a and V_c stand for the volume of anode and cathode respectively.

The water diffusion flow and the electro-osmotic drag through the membrane (i.e.: F_{H2Od} and F_{H2Oeod}) are determined in the membrane ancillary. These parameters are required to complete the mass balance calculation in the anode and cathode, and can be obtained as in [32].

$$F_{H2Od} = D_w \cdot \frac{C_{wc} - C_{wa}}{t_m} \cdot M_{H2O} \cdot A \cdot n_c \tag{9}$$

$$F_{H2Oeod} = n_d \cdot \frac{i}{F} \cdot M_{H2O} \cdot A \cdot n_c \tag{10}$$

In Eq. (9), D_w is the water diffusion coefficient, C_{wc} and C_{wa} are the water concentration for the cathode and anode surface of the membrane respectively, t_m the membrane thickness, M_{H2O} stands for the water molecular weight, while A is the active area of the cell. Regarding Eq. (10), n_d is the electro-osmotic drag coefficient, and i corresponds to the current density in the EZ. More detail about these parameters can be found in [32].

The hydrogen molar flow outputted from the cathode (F_{H2co}, mol/s) in model C is given by Eq. (11), where y_{H2} is the hydrogen molar fraction, k_{co} is an adjustable parameter that accounts for the flow coefficient, P_c is the total cathode pressure, and P_0 is the output pressure of the cathode. Furthermore, the hydrogen production in Nm^3/h can be determined by combining F_{H2co} with the ideal gas law.

$$F_{H2co} = y_{H2} \cdot k_{co} \cdot \left(P_c - P_0\right) \tag{11}$$

The voltage ancillary computes the EZ voltage in this model from three different terms, as shown in Eq. (12), where E is the open circuit voltage, V_{act} is the activation overvoltage, and V_{ohm} is the ohmic overvoltage. Moreover, Eqs. (13)-(15) allow estimating these parameters as in [32].

$$V_{EZ} = E + V_{act} + V_{ohm} \tag{12}$$

$$E = E_0(T) + \frac{R \cdot T}{2 \cdot F} \cdot \ln\left(\frac{p_{H2} \cdot p_{O2}^{1/2}}{a_{H2O}} \right) \tag{13}$$

$$V_{act} = \frac{R \cdot T}{2 \cdot \alpha \cdot F} \cdot \ln\left(\frac{i}{i_0} \right) \tag{14}$$

$$V_{ohm} = I_{EZ} \cdot R_{ohm} \tag{15}$$

E_0 is the standard potential, which can be calculated as a function of the EZ temperature, as given in [33, 34]. Furthermore, a_{H2O} stands for the water activity in the anode, α is the charge transfer coefficient, and i_0 is the reference exchange current density. Finally, R_{ohm} is the membrane resistance, calculated as the ratio between the membrane thickness and its conductivity.

The previous expressions are implemented in the voltage ancillary of the EZ model, thus obtaining the EZ voltage as an output to link this device with the wind turbine in the hybrid system.

3.4. Electrolyzer model D

For the sake of comparison, the alternative EZ model proposed in [35] is taken here as a reference for model D. Subsequently, this is the most detailed configuration amongst the four options observed herein.

Similarly to the previous model, model D is structured into four ancillaries. The anode and cathode ancillaries perform analogous operation. Their main function is to provide the oxygen and hydrogen concentration respectively, apart from their contribution to the water concentration in the membrane channels. This can be achieved

using Eqs. (16)-(19), where subscripts *an* and *cat* stand for anode and cathode, and *ch* for the membrane channels. Hence, C_{O2ch} and C_{H2ch} are the oxygen and hydrogen concentrations in the anode and cathode respectively, carried to the membrane channels; whereas $C_{H2Oan,ch}$ and $C_{H2Ocat,ch}$ denote the contribution to the membrane channels of water concentration from anode and cathode. The molar fractions of oxygen and hydrogen in the channels are expressed as $y_{O2an,ch}$ and $y_{H2cat,ch}$; while the water density ρ_{H2O} appears as a function of the temperature.

$$C_{O2ch} = \frac{P_{an} \cdot y_{O2an,ch}}{R \cdot T} \tag{16}$$

$$C_{H2Oan,ch} = \frac{\rho_{H2O}(T)}{M_{H2O}} \tag{17}$$

$$C_{H2ch} = \frac{P_{cat} \cdot y_{H2cat,ch}}{R \cdot T} \tag{18}$$

$$C_{H2Ocat,ch} = \frac{\rho_{H2O}(T)}{M_{H2O}} \tag{19}$$

The membrane ancillary determines the water flow through the membrane, accounting for the pressure gradient, the electro-osmotic drag, and the diffusion effects. Additionally, the partial pressures of oxygen, hydrogen and water in the membrane (i.e.: p_{O2me}, p_{H2me} and $p_{H2Ome,an}$ respectively) are also computed in this ancillary. These parameters are necessary for the EZ voltage calculation in the voltage ancillary, and can be obtained from Eqs. (20)-(22), where the molar fractions y_{O2me}, y_{H2me} and $y_{H2Ome,an}$ correspond to the conditions of the oxygen, hydrogen and water molecules in the membrane. These magnitudes must be calculated attending to several parameters involved in the electrochemical process, as described in [35].

$$p_{O2me} = y_{O2me} \cdot P_{an} \tag{20}$$

$$p_{H2me} = y_{H2me} \cdot P_{cat} \tag{21}$$

$$p_{H2Ome,an} = y_{H2Ome,an} \cdot P_{an} \tag{22}$$

Regarding the hydrogen generation, this parameter is obtained through Eq. (6), proportionally to the EZ current and the number of series cells, as in model B.

Four terms are employed in Eq. (23) to compose the total EZ voltage in the voltage ancillary of model D. The expression for the open circuit voltage is given in Eq. (24), where E_0 is a function of temperature [33].

$$V_{EZ} = E + V_{act} + V_{ohm} + V_{diff} \tag{23}$$

$$E = E_0(T) + \frac{R \cdot T}{2 \cdot F} \cdot \ln\left(\frac{p_{H2me} \cdot p_{O2me}^{1/2}}{p_{H2Ome,an}} \right) \tag{24}$$

$$V_{act} = \frac{R \cdot T}{\alpha_{an} \cdot F} \cdot \operatorname{arcsinh}\left(\frac{i}{2 \cdot i_{0an}} \right) + \frac{R \cdot T}{\alpha_{cat} \cdot F} \cdot \operatorname{arcsinh}\left(\frac{i}{2 \cdot i_{0cat}} \right) \tag{25}$$

$$V_{ohm} = I_{EZ} \cdot R_{ohm} \tag{26}$$

$$V_{diff} = V_{diff,an} + V_{diff,cat} = \frac{R \cdot T}{4 \cdot F} \cdot \ln\left(\frac{C_{O2me}}{C_{O2me,0}} \right) + \frac{R \cdot T}{2 \cdot F} \cdot \ln\left(\frac{C_{H2me}}{C_{H2me,0}} \right) \tag{27}$$

The activation overvoltage in Eq. (25) can be computed as the sum of this effect in anode and cathode. As a consequence, it is necessary to introduce the charge transfer coefficient in both elements (α_{an} and α_{cat}), as well as their exchange current density

references (i_{0an} and i_{0cat}) [33, 36]. Additionally, the ohmic overvoltage is calculated through Eq. (26), analogously to the strategy followed in model C.

The last term in Eq. (23) corresponds to the diffusion overvoltage, reproduced in Eq. (27), where C_{O2me} and C_{H2me} represent the oxygen and hydrogen concentration at the membrane-electrode interface, and subscript *0* denotes a working condition taken as reference [35]. The bulk concentration of these species is frequently chosen as this reference value [37]. With the aim of achieving a deeper insight in this model, the diffusion overvoltage is evaluated at anode and cathode separately, and then added to the rest of mechanisms considered.

3.5. Validation of models

All the EZ models previously presented have been implemented in MATLAB/Simulink, in order to study their performance when becoming a part of a hybrid system. Prior to this comparative analysis, it is crucial to validate the adequate response of every model, and confirm that their behaviour resembles sufficiently that of a real device. This validation will accredit the results obtained through simulation of the hybrid system.

Subsequently, a commercial device has been chosen as a reference. In the works from Marangio *et al.* [35, 37], the authors provide the polarization curves of a commercial PEM EZ employed on their research. These curves have been obtained under different conditions of pressure and temperature. Therefore, the response of the real device collected from [35, 37] is used here as a benchmark. The variation of voltage and hydrogen production with the input current density in the EZ will be evaluated for the four models.

First, the hydrogen production is shown in Fig. 1a. The EZ working pressure is 10 bar, and its temperature 55 ºC. Only two operational points of the real device are available for this parameter in [35, 37]. Nonetheless, the variation of hydrogen with current in a PEM EZ is commonly considered linear. Hence, only two points can be enough for these validation purposes. As seen, all the models show a linear response that reproduces adequately the operating conditions provided by the manufacturer.

The polarization curves shown in Fig. 1b were obtained under the same pressure and temperature conditions. It is important to remark that all the models considered here present several adjustable parameters that must be fine-tuned *ad hoc*. Therefore, these parameters have been tuned specifically to reproduce the polarization curve of the commercial EZ under these pressure and temperature conditions. Subsequently, it can be noticed that the four models convincingly match the experimental results of the commercial device. More specifically, models C and D achieve a high accuracy even for low current densities. Additionally, identical response was obtained for models A and B, which replicate the polarization curve as a linear function with sufficient precision.

Maintaining the tuning parameters in models B, C and D, an additional test was carried out under a 70 bar pressure and 40 ºC temperature. As detailed before, model A does not consider pressure and temperature variations. Hence, it was necessary to re-tune the adjustable parameters in model A for the new operating conditions of the EZ. As seen in Fig. 1c, all models achieved satisfactory results. Again, it is model D that best approaches the response of the real device. Model C shows a slight deviation from the reference values, but still resembles reasonably well the behaviour of the commercial EZ. Moreover, models A and B provide a positive linear estimation, with the peculiarity that model A needs to be modified according to the working conditions.

Fig. 1. a) H_2 production @ 10bar – 55ºC; b) Polarization curves @ 10bar – 55ºC; c) Polarization curves @ 70bar – 40ºC

Once the models have been validated through comparison against a real device, their coupled operation in a hybrid system will be evaluated later on.

4. Wind hybrid system modelling

The hybrid system modelled herein consists in the coupled operation of a DFIG-driven wind turbine and a PEM EZ, as shown in Fig. 2. The configuration proposed in this paper makes use of the power converter of the DFIG to connect the EZ. In order to adapt the variable DC voltage of the EZ to the constant 2000 V at the DFIG DC bus, a DC/DC converter becomes necessary. This converter, apart from serving as a link between both devices, allows controlling the power transfer to the EZ according to a previously calculated reference.

Moreover, the SCS is responsible for setting the following reference signals: The active power to be consumed in the EZ through the DC/DC converter, and generated by the DFIG via the RSC; the reactive power references for the stator and GSC of the DFIG, as well as the DC bus voltage in the GSC. This structure is shown in Fig. 2, where the reference signals of the SCS are indicated with the superscript '*'. Hence, the SCS implements the coordinated control strategy that governs the performance of the hybrid system.

Fig. 2. Complete scheme of the hybrid system

4.1. DC/DC Converter modelling and control

Provided that the EZ and the DC bus of the DFIG operate under different voltage characteristics, the DC/DC converter presents a valid method to connect both elements. It has been modelled using two IGBT-diode power switches, plus a high frequency inductor that filters the input current, and a filtering capacitor for the output voltage. This structure allows an adequate active power flow to the EZ.

Furthermore, a control strategy must be implemented to drive the duty cycle of the power switches of this converter. Here, the control concept is based on the regulation of the active power consumption in the EZ. As previously stated, the SCS calculates the reference for the active power flow from the DC bus to the EZ. Using a single PI-based control loop, the DC/DC converter is controlled to follow this active power reference, thus enabling the EZ to consume the active power surplus regarding the varying conditions of the wind power system and the grid demand.

4.2. Supervisory Control System

In the hybrid configuration proposed, a control system that coordinates the operation of the DFIG and the EZ becomes necessary. This task is carried out by the SCS, which sets the active and reactive power references for both devices, in order to fulfil the variable grid demands. Hence, two different subsystems can be observed, i.e.: the Active and the Reactive Power SCS. The main aspects of both schemes are described below.

4.2.1. Active power SCS

The main benefit of the coordinated operation of a wind power system coupled with an ESS relies on the ability to manage the active power supply to grid regardless of the incoming wind conditions. The characteristics of the ESS limit to what extend this hybrid system is able to adapt to an externally imposed set-point. For instance, a battery ESS could provide an additional active power injection for hours, whereas an ultracapacitor ESS is more adequate for short power boosts to grid.

In this paper, an ESS based on the hydrogen technology has been considered. In the proposed scheme, a PEM electrolyzer is connected to a DFIG. As a consequence, the ESS is only able to store energy, since the active power flow in this device is unidirectional. This characteristic hinders the capacity to provide active power to grid above the actual generation of the wind power system. Nonetheless, the energy consumed in the EZ is used to generate hydrogen, which can then be stored in a pressurized tank. This tank can be sized to store large amounts of hydrogen. Moreover, it could be emptied without the necessity to stop the input hydrogen flow from the EZ. This ability means that the EZ shows no constraints regarding its state-of-charge, contrarily to what can be observed in other ESS. In conclusion, the EZ is able to absorb active power for as long as necessary.

Taking the previous considerations into account, the active power SCS has been designed to dispatch to the EZ the active power mismatch between the grid demand and the DFIG generation. A limitation has been imposed to avoid reference values that demand active power from the EZ, since only zero output or power consumption are allowed in the EZ. As previously stated, no state-of-charge boundaries have been considered in this configuration.

4.2.2. Reactive power SCS

The capacity to manage the reactive power generation is an important advantage of DFIGs when compared to other wind generation technologies. This characteristic has been implemented in the hybrid system. Given the structure of the DFIG, two different elements to exchange reactive power appear. The stator windings are able to absorb or provide reactive power depending on the current operating conditions of the generator. Moreover, the GSC is also capable of exchanging reactive power with the grid. These parameters are controlled in the RSC and GSC control schemes, as previously described. The reactive power SCS is responsible for setting the reactive power references for both devices in the proposed hybrid configuration.

Both the stator and GSC show certain current boundaries that limit the reactive power flow. The reactive power SCS implemented evaluates these constraints dynamically to achieve a proportional reactive power dispatch. With this strategy, the total reactive power supply/consumption will be distributed between both elements proportionally to their instantaneous capacity. The stator availability can be determined as a function of certain operating conditions of the DFIG. As depicted in [38], the rotor current and voltage, as well as the stator current, define the active-reactive power curve of the generator. The maximum apparent power through the stator windings regarding these limiting parameters (i.e.: S_{s_Ir}, S_{s_Vr} and S_{s_Is} respectively) can be obtained through Eqs. (28)-(30), where S is apparent power, V is voltage, I stands for current, Z for impedance and *slip* is the DFIG slip; and subscript s is used for stator, r for rotor and m for mutual.

$$S_{s\_Ir} = -U_s \cdot U_s^* \cdot \left(\frac{1}{Z_s + Z_m} \right)^* + I_r^* \cdot U_s \cdot \left(\frac{Z_m}{Z_s + Z_m} \right)^* \tag{28}$$

$$S_{s\_Vr} = -U_s \cdot \left(\frac{U_s \cdot \left(Z_r + Z_m \right) - \frac{U_r}{slip} \cdot Z_m}{\left(Z_r + Z_s \right) \cdot Z_m + Z_s \cdot Z_r} \right)^* \tag{29}$$

$$S_{s\_Is} = -U_s \cdot I_s^* \tag{30}$$

In the hybrid system model, the stator reactive power consumption and generation limits are chosen as the lowest absolute value from the three positive and three negative results obtained from Eqs. (28)-(30), respectively.

The reactive power restrictions in the GSC can be calculated regarding the nominal power of the converter (S_{nom}). Prioritizing the active power flow through the GSC (P_{gsc}), the reactive power limitations (Q_{gsc_lim}) are given by Eq. (31), where the positive and negative signs correspond to the consumption and generation boundaries respectively.

$$Q_{gsc\_lim} = \pm \sqrt{S_{nom}^2 - P_{gsc}^2} \tag{31}$$

The total reactive power requirements of the hybrid system are distributed by the SCS between stator and GSC proportionally to their availability [25]. Eq. (32) shows the calculation of the stator reactive power reference (Q_{s_ref}). As seen, the stator covers a fraction of the total reactive power demand (Q_{dem}) corresponding to the ratio between the stator and the total reactive power limitations ($Q_{s\_con\_lim}$ and $Q_{con\_lim\_total}$ respectively, where subscript *con* stands for consumption, and *lim* for limit). Furthermore, the total

boundaries of the hybrid system are the sum of the stator and GSC ($Q_{gsc\_con\_lim}$) disposable reactive power, as in Eq. (33). In Eqs. (32) and (33), only the case for reactive power consumption in the stator is shown. However, analogous expressions are used for reactive power generation, and also for the GSC. Through this strategy, the grid reactive power demand can be completely addressed as long as it remains within the maximum operating points of the hybrid system.

$$Q_{s\_ref} = \frac{Q_{s\_con\_lim}}{Q_{con\_lim\_total}} \cdot Q_{dem\ (con)} \tag{32}$$

$$Q_{con\_lim\_total} = Q_{s\_con\_lim} + Q_{gsc\_con\_lim} \tag{33}$$

5. Simulations and discussion

After validating the EZ models in Section 3.5, the performance of the four configurations considered has been studied through simulation of the hybrid system. The EZ models coupled to the DFIG based wind turbine have been evaluated under fluctuating wind speed and variable active and reactive power grid demand. This scenario embraces very challenging working conditions of the hybrid system during normal grid-connected operation. Furthermore, it allows examining the adequate response of the control systems implemented.

As stated before, a fluctuating wind speed time series was inputted to the wind turbine model. As seen in Fig. 3, the wind speed remains above the rated value of the generator during the first 115 s, and then fluctuates mostly below the rated value for the rest of the simulation. The active power generation of the DFIG (P_g) responds accordingly, producing the nominal value of 1 pu for above rated wind speed, and

varying with the wind speed for below rated values. The DFIG power generation P_g does not depend on the EZ model, as shown in Fig. 4a.

Fig. 3. Wind speed

The active power demanded by the grid was set in three different levels. From 0 to 80 s, the grid demanded 0.7 pu from the hybrid system. At 80 s this value increased to 1 pu with a rising slope of 0.5 pu/s, and remained at this state until 160 s, when it decreased at a rate of -0.5 pu/s to 0.5 pu, which was maintained up to the end of the simulation. It is not reasonable to set a grid demand above the rated power of the DFIG in the hybrid system under study, since fuel cells have not been included in the scheme, thus being only able to store energy in the EZ.

Fig. 4b shows the total active power generated by the hybrid system (P_t). It can be clearly seen that the hybrid configuration adapts to the grid requirements during most of the simulation. Exclusively between 115 and 160 s the demand is not addressed. During this period, the grid requested 1 pu, whereas the input wind speed is lower than the DFIG rated value. As a consequence, P_g falls below its nominal generation, and since the EZ can only absorb power, the grid requirements remain unfulfilled. For the rest of the simulation, the hybrid system provides the grid with the commanded amount of active power. This can be achieved by storing in the EZ the power surplus when the DFIG generation exceeds the grid requirements. Hence, flexible active power generation has been accomplished in the hybrid system by means of the EZ.

It is also remarkable in Fig. 4b that the total active power generation recorded was similar for the four EZ models compared. No noticeable differences can be observed for this parameter between the four options presented. This fact is reinforced in Fig. 4c, where the active power delivered to the EZ models (P_{EZ}) is illustrated. Here, it can be stressed that all EZ models perform analogously. During the first 80 s, the EZs absorb 0.3 pu due to the power mismatch between DFIG generation and demand. From 80 to 160 s the power consumed in the EZs is zero, since no excess wind power appears. Eventually, the EZs input fluctuates as a result of the variations in the DFIG output power.

Fig. 4. a) DFIG active power generation; b) Total active power generation; c) EZ active power consumption

Regarding the reactive power grid demand, it is set at -0.6 pu until 120 s, when it switches to 0.45 pu with a rate of 0.1 pu/s, thus covering a wide range of operation varying from reactive power generation to consumption (negative and positive values respectively). The response of the models implemented is shown in Fig. 5. It can be appreciated that the reactive power SCS delivers the grid requirements between stator and GSC proportionally to their availability. As a result, the grid demand can be completely fulfilled during the whole simulation. Since only active power can be exchanged with the EZs, the performance of all models is equivalent as expected, and their representations overlap in Fig. 5.

Fig. 5. a) Total reactive power output: b) Stator reactive power output; c) GSC reactive power output

Looking into the most representative parameters of the EZ models, Fig. 6 illustrates the voltage, current and hydrogen generation output from each model (i.e.: V_{EZ}, I_{EZ} and n_{H2} respectively). Certain dissimilarities can be foreseen for these signals, provided that their correspondence was not always exact in Fig. 1. Hence, it can be appreciated in Fig. 6a that only models A and B show the same voltage profile, whereas models C and D do not match completely. Moreover, it can be observed in Fig. 6a that the disparity between models C and D reaches its maximum for low EZ currents (from 80 to 160 s, as seen in Fig. 6b); while it is minimum between D, A and B during this interval. For the rest of the simulation, the distance between the different models varies as a function of the EZ current, in accordance with Fig. 1b. Nonetheless, it can be clearly noticed that all responses follow a similar tendency throughout the simulation.

The EZ current response, illustrated in Fig. 6b, resembles the active power registered in this device, represented in Fig. 4c. As seen, a constant current is observed up to 80 s, when it becomes zero as the power absorption in the EZ ceases. From 160 s on, a variable power supply to the EZ translates into a changing current flow in this device. The same occurs with the hydrogen production depicted in Fig. 6c. A constant current injection of approximately 370 A results in 60 Nm^3/h of hydrogen generated. Accordingly, this parameter fluctuates during the last simulation interval, reaching a maximum peak of 100 Nm^3/h at 160 s, coinciding with a peak current of 600 A into the EZ. Furthermore, the hydrogen output is zero from 80 to 160 s. Only model C registers a value of 3 Nm^3/h during this period, since the hydrogen production is not directly

proportional to the EZ current in this model, but it is determined as a function of several parameters. As a result, this response is not numerically zero, but it shows a clear tendency towards this value.

Fig. 6. a) EZ voltage; b) EZ current; c) EZ hydrogen generation

Finally, it is important to scan the voltage measured at the DC bus of the DFIG during the simulation. As detailed before, the EZ is connected to the DFIG DC bus in the configuration evaluated. As a consequence, it is necessary to confirm that the active power flow to the EZ does not have a negative influence on the bus voltage, which could hamper the adequate operation of the wind turbine. Fig. 7 demonstrates the proper performance of the DC voltage controller throughout this experience. For every model studied, the DC voltage remains stable at 2000 V, even when the active power exchange fluctuates during the last simulation period.

Fig. 7. Voltage at the DC bus of the DFIG

6. Conclusions

In order to strengthen the growth of renewable energies, the deployment of hybrid systems is regarded as a feasible alternative that gathers the benefits from the several power sources involved. In this regard, the use of EZs appears as an ideal option to

profit from the excess wind power that otherwise would be curtailed and wasted. These devices can produce hydrogen from the generation surpluses in a wind farm. The hydrogen generated can be used later on as an energy carrier for electricity generation in fuel cells, for transportation in different vehicles, or in the chemical industry. The modelling of such hybrid systems has been addressed in this paper. Four different EZ models, which have been thoroughly described, have been studied for their integration with a DFIG driven wind turbine. The behaviour of these hybrid systems has been evaluated through simulation.

The simulation results have shown a satisfactory coordinate operation between the wind turbine and all the EZ models, facilitated by the SCS implemented. As previously described, the four EZ models subject of this study performed similarly under fluctuating wind speed and variable active and reactive power grid demand, achieving an adequate electrical response in all cases. The results showed no critical deficiencies that allowed rejecting any of the models. Subsequently, the decision to use one EZ model or another relies mostly on the characteristics of the application under study, since all of them perform analogously in dynamic hybrid systems simulations, such as the one evaluated in this paper. Therefore, when detailed information about the internal processes of the EZ is of interest for the analysis, either model C or D can be implemented, whereas when only the electrical response is necessary, EZ models A and B provide a much simpler tool for the analysis. Between models A and B, it is important to highlight that option A does not offer the possibility to vary pressure and temperature conditions (opposite to model B, where this possibility is available). In such case, it is necessary to recalculate the model parameters in model A, thus preventing the use of this model for applications where variations of pressure and temperature in the EZ must be contemplated. Regarding models C and D, a much longer computation time has been

registered for model C. This inconvenience, together with the inaccuracy to calculate the hydrogen generation under zero current conditions observed in the simulation, and the deviation from the commercial device for variable pressure and temperature conditions observed in Fig. 1c, favours the use of model D in detailed studies of the EZ performance in hybrid systems.

Acknowledgements

This work has been supported by the University of Cadiz under the Grant FPI 2012-036, and by the Spanish Ministry of Science and Innovation under Grant ENE2010-19744/ALT.

References

[1] Nehrir MH, Wang C, Strunz K, Aki H, Ramakumar R, Bing J, et al. A Review of Hybrid Renewable/Alternative Energy Systems for Electric Power Generation: Configurations, Control, and Applications. IEEE Trans Sustain Energy 2011;2:392-403.

[2] Mohammed YS, Mustafa MW, Bashir N. Hybrid renewable energy systems for off-grid electric power: Review of substantial issues. Renew Sust Energy Rev 2014;35:527-39.

[3] Moslehi K, Kumar R. A Reliability Perspective of the Smart Grid. IEEE Trans Smart Grid 2010;1:57-64.

[4] Luna-Rubio R, Trejo-Perea M, Vargas-Vazquez D, Rios-Moreno GJ. Optimal sizing of renewable hybrids energy systems: A review of methodologies. Sol Energy 2012;86:1077-88.

[5] Díaz-González F, Sumper A, Gomis-Bellmunt O, Villafáfila-Robles R. A review of energy storage technologies for wind power applications. Renew Sustain Energy Rev 2012;16:2154-71.

[6] Sherif SA, Barbir F, Veziroglu TN. Wind energy and the hydrogen economy—review of the technology. Sol Energy 2005;78:647-60.

[7] Akinyele DO, Rayudu RK. Review of energy storage technologies for sustainable power networks. Sustain Energy Technol Assess 2014;8:74-91.

[8] Evans A, Strezov V, Evans TJ. Assessment of utility energy storage options for increased renewable energy penetration. Renew Sustain Energy Rev 2012;16:4141-7.

[9] Hasan NS, Hassan MY, Majid MS, Rahman HA. Review of storage schemes for wind energy systems. Renew Sustain Energy Rev 2013;21:237-47.

[10] Gahleitner G. Hydrogen from renewable electricity: An international review of power-to-gas pilot plants for stationary applications. Int J Hydrogen Energy 2013;38:2039-61.

[11] Mathiesen BV, Lund H. Comparative analyses of seven technologies to facilitate the integration of fluctuating renewable energy sources. IET Renew Power Gener 2009;3(2):190-204.

[12] Ridjan I, Mathiesen BV, Connolly D. Synthetic fuel production costs by means of solid oxide electrolysis cells. Energy 2014;76:104-13.

[13] Connolly D, Mathiesen BV, Ridjan I. A comparison between renewable transport fuels that can supplement or replace biofuels in a 100% renewable energy system. Energy 2014;73:110-25.

[14] Uzunoglu M, Onar OC, Alam MS. Modeling, control and simulation of a PV/FC/UC based hybrid power generation system for stand-alone applications. Renew Energy 2009;34:509-20.

[15] Hwang JJ, Lai LK, Wu W, Chang WR. Dynamic modeling of a photovoltaic hydrogen fuel cell hybrid system. Int J Hydrogen Energy 2009;34:9531-42.

[16] Carr S, Premier GC, Guwy AJ, Dinsdale RM, Maddy J. Hydrogen storage and demand to increase wind power onto electricity distribution networks. Int J Hydrogen Energy 2014;39:10195-207.

[17] Zhou T, Francois B. Modeling and control design of hydrogen production process for an active hydrogen/wind hybrid power system. Int J Hydrogen Energy 2009;34:21-30.

[18] Ulleberg Ø, Nakken T, Eté A. The wind/hydrogen demonstration system at Utsira in Norway: Evaluation of system performance using operational data and updated hydrogen energy system modeling tools. Int J Hydrogen Energy 2010;35:1841-52.

[19] Carton JG, Olabi AG. Wind/hydrogen hybrid systems: Opportunity for Ireland's wind resource to provide consistent sustainable energy supply. Energy 2010;35:4536-44.

[20] Tao Z, Francois B. Energy Management and Power Control of a Hybrid Active Wind Generator for Distributed Power Generation and Grid Integration. IEEE Trans Ind Electron 2011;58:95-104.

[21] Sanchez I, Ursua A, Marroyo L, Sanchis P. Primary regulation strategies applicable to wind farms coupled with hydrogen production systems. International Conference on Clean Electrical Power (ICCEP), 2011. p. 584-7.

[22] Muyeen SM, Takahashi R, Tamura J. Electrolyzer switching strategy for hydrogen generation from variable speed wind generator. Electr Power Syst Res 2011;81:1171-9.

[23] General Electric Company. Products & Services: 1.5 - 77 Wind Turbine <http://site.ge-energy.com/prod_serv/products/wind_turbines/en/15mw/index.htm> [accessed 12.10.14]

[24] Sarrias R, Fernandez LM, Garcia CA, Jurado F. Coordinate operation of power sources in a doubly-fed induction generator wind turbine/battery hybrid power system. J Power Sources 2012;205:354-66.

[25] Sarrias-Mena R, Fernández-Ramírez LM, García-Vázquez CA, Jurado F. Fuzzy logic based power management strategy of a multi-MW doubly-fed induction generator wind turbine with battery and ultracapacitor. Energy 2014;70:561-76.

[26] Heier S. Grid integration of wind energy conversion systems. John Wiley & Sons; 1998.

[27] Slootweg JG. Wind Power: Modelling and Impact on Power System Dynamics [PhD Thesis]. Netherlands: Delft University of Technology; 2003.

[28] Krause P, Wasynczuk O, Sudhoff S. Analysis of electric machinery and drive systems. IEEE Press series on power engineering. John Wiley & Sons; 2002.

[29] Castañeda M, Cano A, Jurado F, Sánchez H, Fernández LM. Sizing optimization, dynamic modeling and energy management strategies of a stand-alone PV/hydrogen/battery-based hybrid system. Int J Hydrogen Energy 2013;38:3830-45.

[30] Khan MJ, Iqbal MT. Dynamic modeling and simulation of a small wind–fuel cell hybrid energy system. Renew Energy 2005;30:421-39.

[31] Atlam O, Kolhe M. Equivalent electrical model for a proton exchange membrane (PEM) electrolyser. Energy Convers Manag 2011;52:2952-7.

[32] Gorgun H. Dynamic modelling of a proton exchange membrane (PEM) electrolyzer. Int J Hydrogen Energy 2006;31:29-38.

[33] Awasthi A, Scott K, Basu S. Dynamic modeling and simulation of a proton exchange membrane electrolyzer for hydrogen production. Int J Hydrogen Energy 2011;36:14779-86.

[34] Carmo M, Fritz DL, Mergel J, Stolten D. A comprehensive review on PEM water electrolysis. Int J Hydrogen Energy 2013;38:4901-34.

[35] Marangio F, Santarelli M, Cali M. Theoretical model and experimental analysis of a high pressure PEM water electrolyser for hydrogen production. Int J Hydrogen Energy 2009;34:1143-58.

[36] Santarelli MG, Torchio MF, Cochis P. Parameters estimation of a PEM fuel cell polarization curve and analysis of their behavior with temperature. J Power Sources 2006;159:824-35.

[37] Marangio F, Santarelli M, Pagani M, Calì Quaglia M. Direct High Pressure Hydrogen Production: a Laboratory Scale PEM Electrolyser Prototype. ECS Trans 2009;17:555-67.

[38] Lund T, Sørensen P, Eek J. Reactive power capability of a wind turbine with doubly fed induction generator. Wind Energy 2007;10:379-94.

LIST OF FIGURES

Figure 1

Click here to download high resolution image

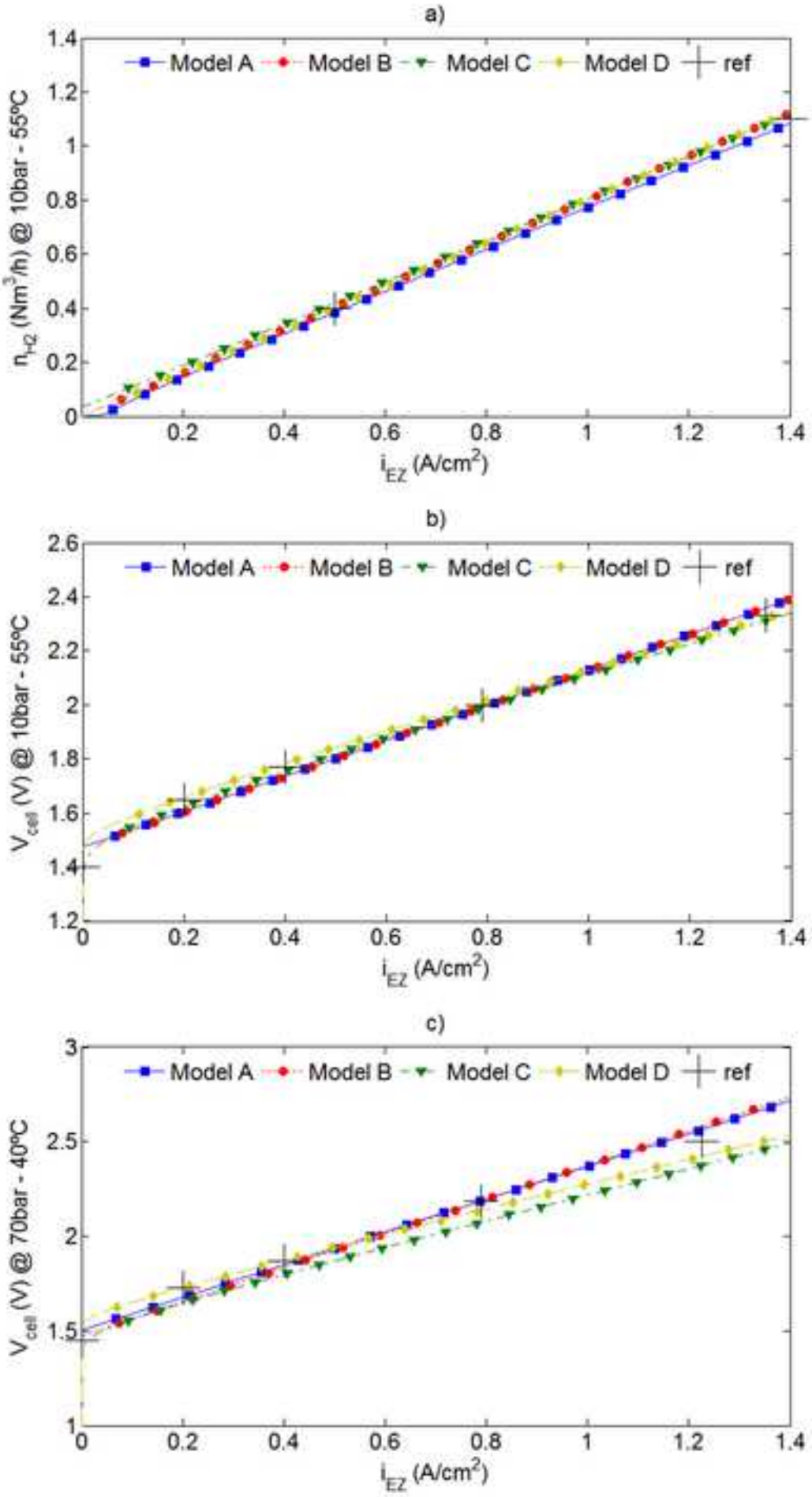

Figure 2

Click here to download high resolution image

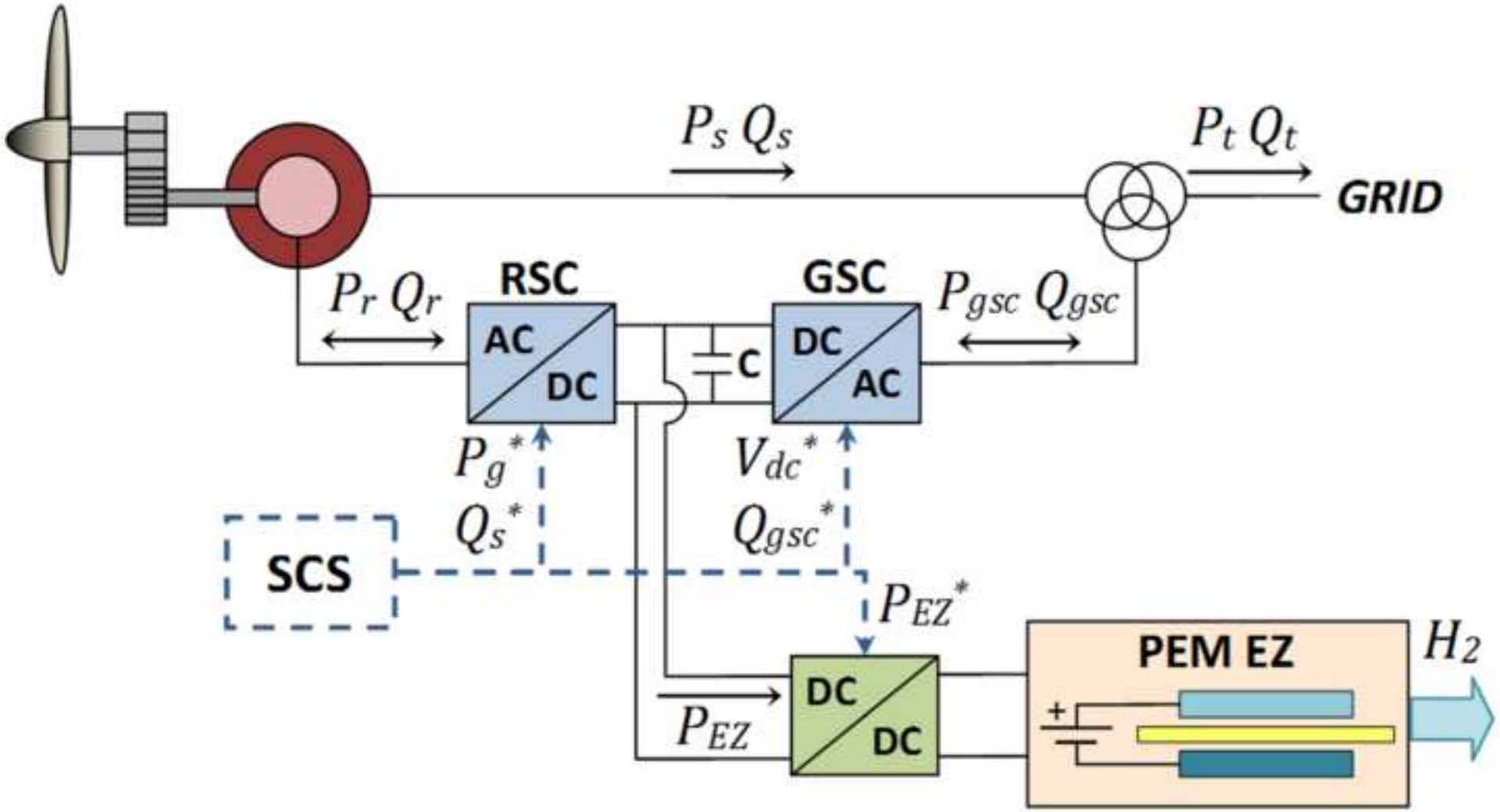

Figure 3

Click here to download high resolution image

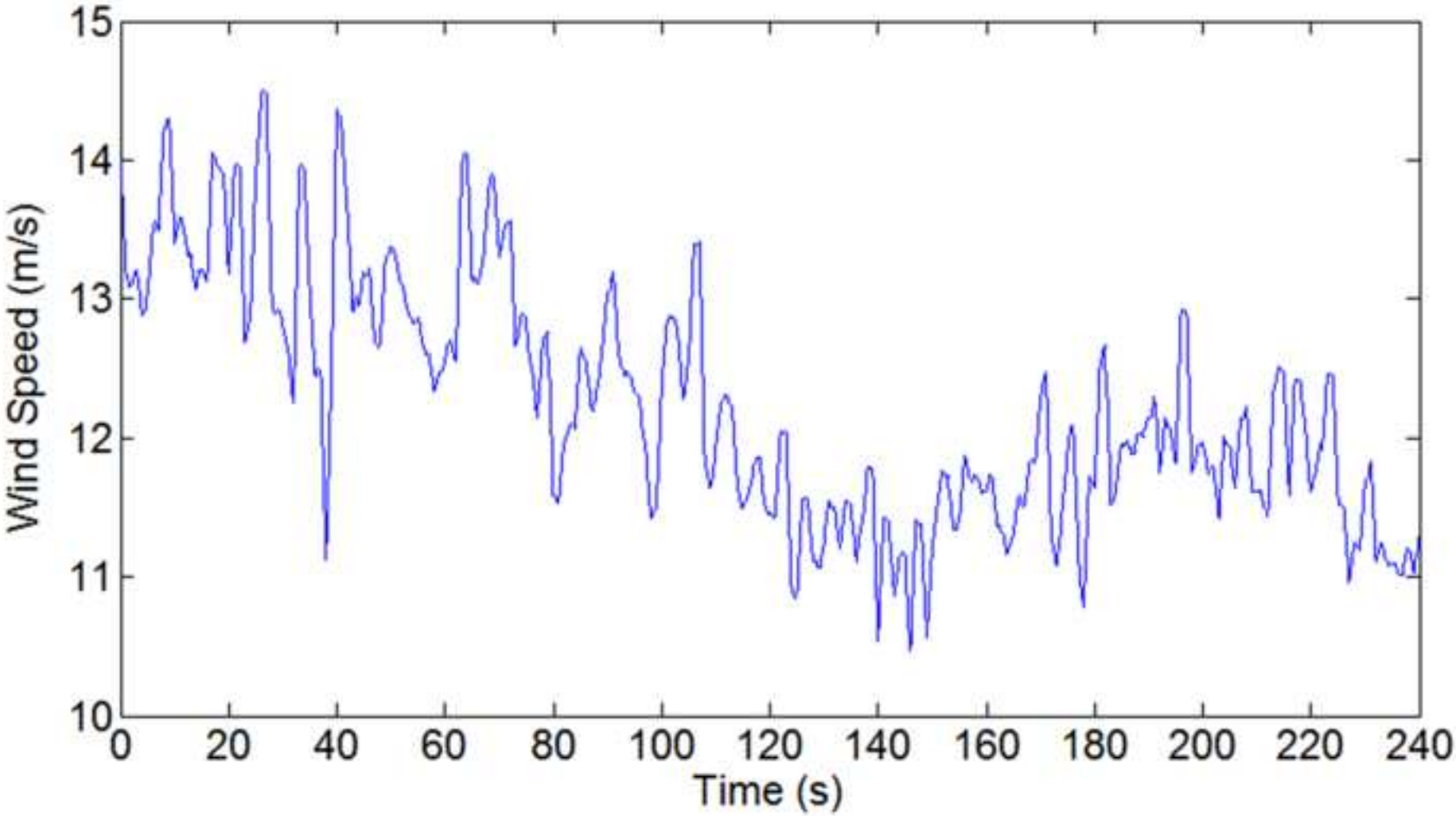

Figure 4

Click here to download high resolution image

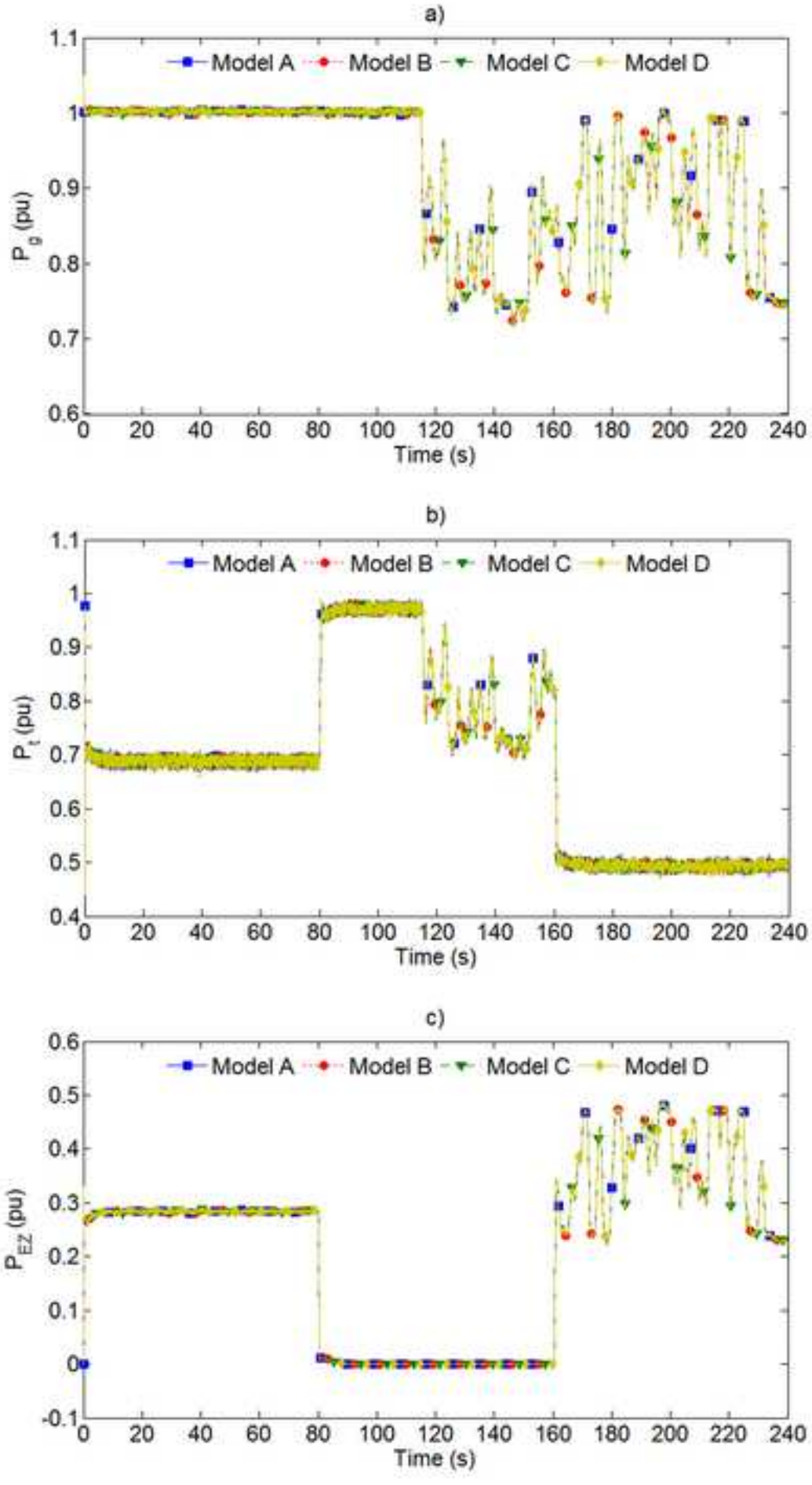

Figure 5

Click here to download high resolution image

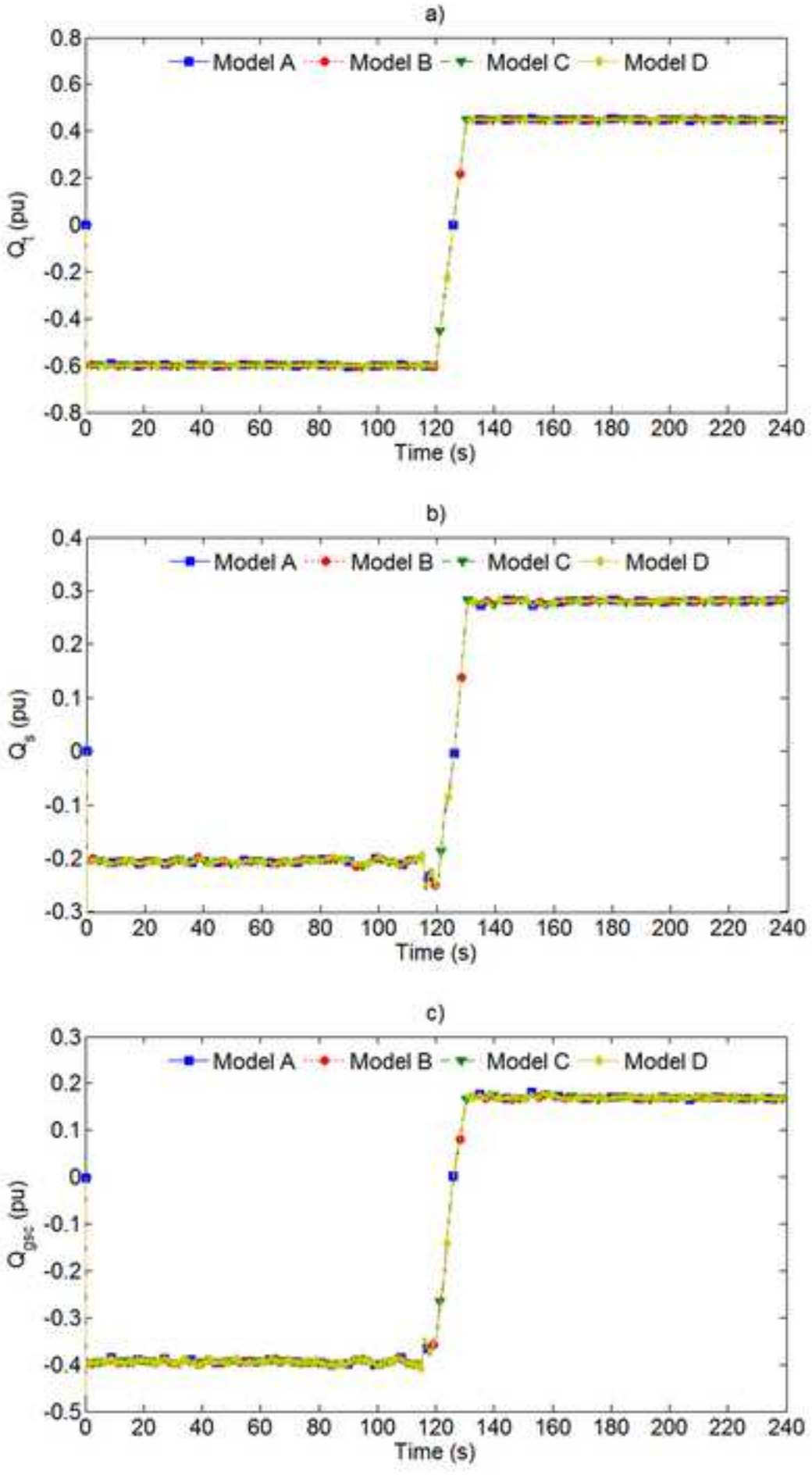

Figure 6

Click here to download high resolution image

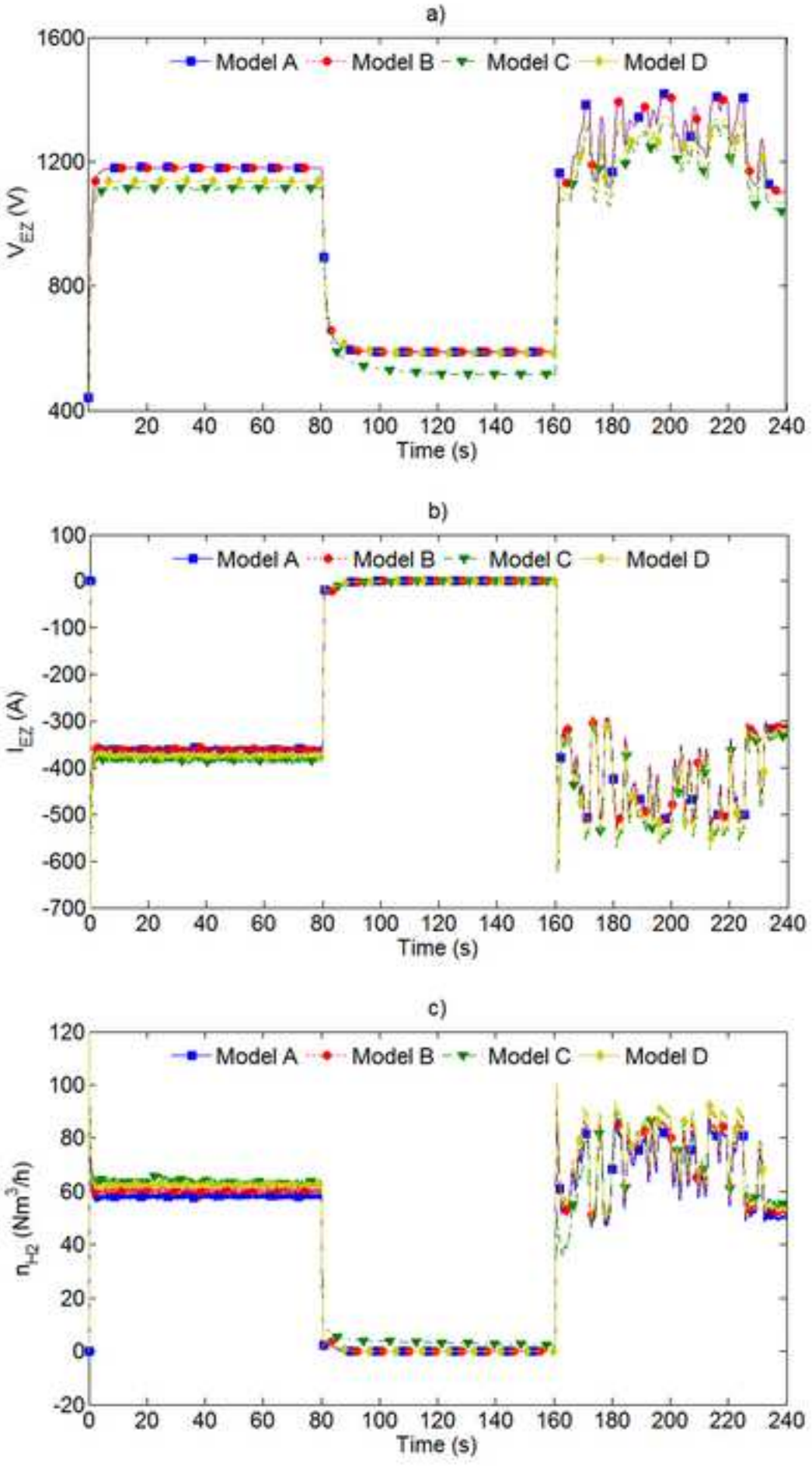

Figure 7

Click here to download high resolution image